J Appl Biomed
DOI: 10.32725/jab.2025.007
journal homepage: http://jab.zsf.jcu.cz

Journal of Applied Biomedicine

Original research article

Berberine improves atrial remodeling by regulating the AMPK/PPARα signaling pathway in a rabbit model of atrial fibrillation

Yang Wang * [a], Zhe Sun [a], Zong-tao Yin, Jian Zhang, Fang-ran Xin, Yin-li Xu, Huai Lan

General Hospital of Northern Theater Command, Department of Cardiovascular Surgery, Shenyang, Liaoning, China

Abstract
Atrial fibrillation (AF) is a common arrhythmia encountered in clinical practice, characterized by myocardial fibrosis and atrial remodeling as its primary pathological features, and associated with significantly high mortality and disability rates. Currently, there are no specific pharmacological treatments for AF, and traditional anti-arrhythmic drugs have not achieved the desired efficacy, often resulting in a high incidence of adverse drug reactions. Thus, there is an urgent need for the development of novel anti-AF medications. Berberine, the main active component of *Coptis chinensis*, has been shown to have antiarrhythmic and anti-heart failure effects. However, its potential to improve atrial fibrosis and remodeling resulting from AF remains largely unexplored. In this study, we used a rapid atrial pacing (RAP) procedure to establish a rabbit model of AF associated with atrial fibrosis. Our objective was to assess the inhibitory effects of berberine on myocardial fibrosis, evaluate its impact on atrial remodeling, and investigate its underlying molecular mechanisms. Our findings indicate that berberine reduces left atrial weight and the area of myocardial fibrosis, inhibits the expression of α-SMA protein in atrial tissue, and decreases the levels of inflammation and oxidative stress. In addition, berberine effectively inhibits atrial remodeling, which may contribute to the prevention of AF. Through transcriptomics, molecular docking, and molecular dynamics simulations, we have tentatively confirmed that berberine may activate the AMPK-PPARα signaling pathway by directly binding to AMPK and PPARα, thereby improving atrial fibrillation.

Keywords: AMPK-PPARα pathway; Atrial fibrillation; Atrial remodeling; Berberine; Rapid atrial pacing

Highlights:
- Berberine effectively inhibits atrial remodeling, which contributes to the prevention of AF.
- Berberine inhibits the expression of α-SMA protein in atrial tissue, and decreases the levels of inflammation and oxidative stress.
- Berberine may activate the AMPK-PPARα signaling pathway by directly binding to AMPK and PPARα, thereby improving atrial fibrillation.

Introduction

Atrial fibrillation (AF) is one of the most common arrhythmias encountered in clinical practice, and its incidence is rising annually due to the increasing aging of the global population. AF not only severely impairs cardiac function and the quality of life of patients, but also significantly heightens the risk of cardiovascular and cerebrovascular events, including stroke and heart failure (Rillig et al., 2021). In China, the prevalence of AF has shown a marked upward trend alongside the increasing elderly population, with the average prevalence rate reaching 0.65%, a figure expected to continue increasing (Song, 2022). The pathogenesis of AF is complex and remains incompletely understood. Current research indicates that the onset and maintenance of AF are closely associated with atrial remodeling, characterized primarily by atrial enlargement and myocardial fibrosis (Liu et al., 2023b; Shu et al., 2023). These pathological alterations underpin the occurrence and persistence of AF. Myocardial fibrosis, defined as the abnormal proliferation of extracellular matrix (ECM) within the myocardium, results in structural and functional changes in the atria and serves as a critical indicator of AF-related structural remodeling. There are various treatment strategies for AF, including pharmacological therapy, electrophysiological interventions, and surgical options (Brenyo and Aktas 2011). However, current treatment strategies often face challenges such as limited efficacy and notable side effects (Gutierrez and Blanchard 2016). Thus, the pursuit of novel drugs and strategies for the management of AF has emerged as a significant focus of medical research.

* **Corresponding author:** Yang Wang, General Hospital of Northern Theater Command, Department of Cardiovascular Surgery No. 83, Wenhua Rd Shenhe District Shenyang 110847, Liaoning, 110016 China; e-mail: wangyanglk1980@163.com
http://doi.org/10.32725/jab.2025.007
[a] These authors contributed equally to this work.

Submitted: 2025-01-09 • Accepted: 2025-05-26 • Prepublished online: 2025-05-27
J Appl Biomed 23/2: 63–79 • EISSN 1214-0287 • ISSN 1214-021X

Contemporary medical research has demonstrated that berberine (BBR), an ingredient in traditional Chinese medicine, has extensive pharmacological activity (Song et al., 2020). It is mainly found in *Coptis*, *Phellodendron*, and other herbs used in traditional Chinese medicine, exhibiting anti-inflammatory, antioxidant, hypoglycemic, and hypolipidemic effects (Wang et al., 2017a). Recently, significant progress has been made in understanding the role of BBR in the cardiovascular system (Feng et al., 2019). Research indicates that BBR can reduce inflammation, myocardial damage, and arrhythmias, as well as provide myocardial protection (Qing et al., 2018). In particular, the potential therapeutic effects of BBR in the context of AF have garnered considerable attention. Several studies suggest that BBR may alleviate symptoms of AF through various mechanisms, including anti-arrhythmic, anti-inflammatory, and antioxidant activities. For instance, BBR has been shown to prevent the abnormal automatic rhythm of cardiomyocytes, thereby reducing the frequency of AF. Additionally, it appears to mitigate the inflammatory response in cardiac muscle and lower oxidative stress levels, ultimately protecting cardiac muscle cells from damage (Cheng et al., 2022; Jia et al., 2022). However, whether BBR can improve AF-induced atrial fibrosis remains unclear.

Therefore, the objective of this study was to investigate the protective effect of BBR on AF-induced atrial fibrosis and to elucidate its underlying molecular mechanisms. We used a rapid atrial pacing (RAP) procedure to simulate rapid atrial rhythm and establish a rabbit model of AF associated with atrial fibrosis. In addition, we also aimed to examine the effects of BBR on atrial fibrosis, assess its impact on atrial remodeling, and explore its potential molecular mechanisms.

Materials and methods

Reagents and materials

Berberine (BBR) was purchased from Northeast Pharmaceutical Group Shenyang First Pharmaceutical Co., Ltd. (Shenyang, China). The hematoxylin and eosin (H&E) staining kit was purchased from Jiangsu Kaiji Biotechnology Co., Ltd. (Nanjing, China), and the Masson staining kit was purchased from Zhuhai Beso Biotechnology Co., Ltd. (Zhuhai, China). The α-SMA, and GAPDH antibodies were obtained from ImmunoWay Biotechnology Company (Plano, Texas, USA). The AMPK, PPARα, p-AMPK, β-actin antibodies, and the horseradish peroxidase (HRP)-labelled secondary antibody were obtained from Beijing Bioss Biotechnology Co., Ltd. (Beijing, China). The superoxide dismutase (SOD), malondialdehyde (MDA), and myeloperoxidase (MPO) detection kits were obtained from Nanjing Jiancheng Bioengineering Institute (Nanjing, China). The IL-1β, IL-6, and TNF-α enzyme-linked immunosorbent assay (ELISA) kits were obtained from Solarbio Science & Technology Co., Ltd. (Beijing, China). The primers, SteadyPure universal RNA Extraction kit, Evo M-MLV reverse transcription Premix kit, and SYBR Green Pro Taq HS Premix qPCR Kit were purchased from Accurate Biotechnology Co., Ltd. (Changsha, China).

Animal grouping and intervention

Thirty male SPF New Zealand rabbits, each weighing between 2.8 and 3.2 kg, were obtained from Qingdao Kangda Biotechnology Co., Ltd. (Qingdao, China; License No. SCXK (Lu) 2016 0002). The rabbits were housed in the Laboratory Animal Center of Liaoning University of Traditional Chinese Medicine (Shenyang, China), kept at an indoor temperature of 18–24 °C, and humidity level of 55 ± 2%, with *ad libitum* access to water. They were allowed a one-week period for adaptive feeding prior to the experiment. All procedures were performed according to the guidelines of Liaoning University of Traditional Chinese Medicine Institutional Animal Care and Use Committee. This research was approved by Liaoning University of Traditional Chinese Medicine Institutional Animal Care and Use Committee. Rabbits were randomly assigned to five groups: a control group, a sham operation group, a sham operation + BBR group, a RAP model group, and a RAP + BBR model group, with six rabbits in each group. The rabbits in the RAP + BBR group and the sham + BBR group received BBR at a dosage of 100 mg/kg once daily for three weeks, starting one week prior to surgery. The remaining groups were administered equal volumes of saline once daily for the same duration.

Establishment of a rabbit AF model using RAP

New Zealand rabbits received an intramuscular injection of Lubenine II at a dosage of 3–4 mg/kg. Following muscle relaxation, midazolam was administered *via* the auricular vein at a dose of 0.5 mg/kg, which resulted in a diminished corneal reflex and eyelash reflex, complete muscle relaxation, and the absence of agitation, thereby inducing a state of anesthesia in the rabbits. The animals were then placed in supine position on the operating table, with their limbs secured. The incisors were fixed to the upper part of the operating table using a string to ensure an unobstructed respiratory tract. The left chest, left upper abdomen, and bilateral armpits were shaved, disinfected, and covered with cloth. Lidocaine was injected at the incision site to numb the skin and alleviate pain. An incision was made in the skin of the left middle and upper abdomen, and a subcutaneous pouch was created for the placement of implants. Four electrode wires were extended through a subcutaneous tunnel, with small openings created in the skin of both upper limb armpits. The two electrocardiogram (ECG) collecting electrodes were extracted through the subcutaneous tunnel, sutured in place, and positioned beneath the subcutaneous skin in the armpits of both upper limbs. The ECG was monitored to confirm the stability and proper functioning of the implant. Next, an incision was made in the third intercostal space on the left side, and the stimulation electrode was positioned transdermally in the three intercostal muscles. Following the thoracotomy at the third intercostal space, a portion of the pericardium was excised, and pericardial fluid was absorbed using cotton balls. Two stimulation electrodes were attached by suturing to the left atrial appendage, ensuring a minimum distance of 10 mm between them (Fig. 1A–B). Before closing the incision, care was taken to remove any chest clots and residual gas to prevent pneumothorax. Penicillin sodium was administered for infection prophylaxis (400,000 units, intramuscular injection once a day for three consecutive days). The experimental rabbits recovered within three days post-surgery. Following their recovery, the animal telemetry stimulation system was activated, enabling the wireless collection and transmission of stimulation signals. Continuous monitoring of body surface I lead electrocardiogram signals was performed using the PowerLab physiological recorder, while intermittent electrical stimulation was administered using a specialized stimulation software. The specific parameters for stimulation were set as follows: stimulation for 2 seconds, followed by a 2-second pause, a frequency of 20 Hz, an intensity of 2 mA, and a pulse width of 1 ms (Fig. 1C). This protocol was used for a duration of two weeks. Rabbits in the RAP + BBR group and the sham+BBR group received BBR injections for three weeks, starting one week prior to surgery. In contrast, the other groups were administered normal saline (Zhou

et al., 2015). Throughout the experiment, all rabbits remained awake and active, with no changes observed in their eating and sleeping patterns. After the final administration, the rabbits were anesthetized, and the entire left atrial tissue was excised. This tissue was then cleaned with pre-cooled normal saline, and any excess material, including thrombus and cellulose, was removed. A portion of the atrial tissue was fixed and preserved in 4% paraformaldehyde, while the remainder was stored in a freezer at –80 °C. The SOD activity and MDA content were measured using a biochemical kit, while the expression levels of interleukin 1 beta (IL-1β), interleukin 6 (IL-6), and tumor necrosis factor α (TNF-α) were measured using an ELISA kit. All experimental procedures were performed in strict accordance with the manufacturer's instructions.

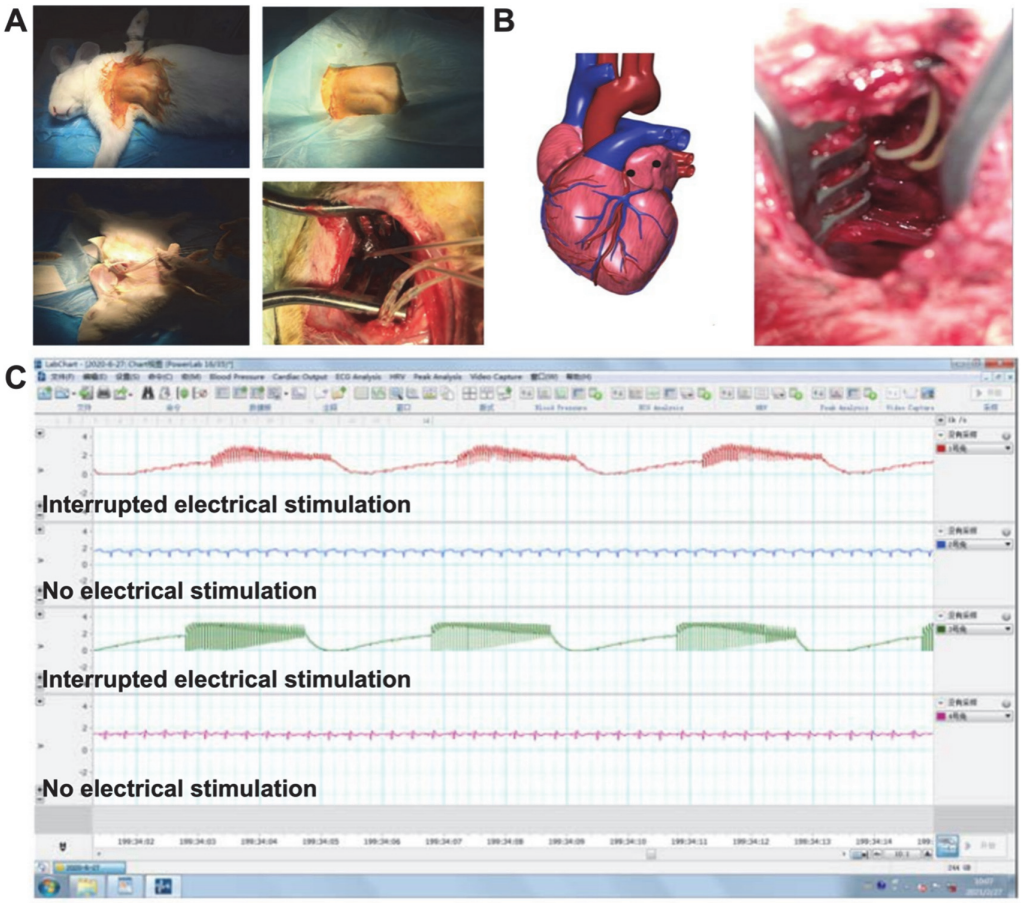

Fig. 1. Establishment of rapid atrial pacing (RAP) rabbit model of atrial fibrillation (AF). (**A**) Representative images of rabbit surgical procedures. (**B**) The suture position of the stimulation electrode and the actual suture position of the stimulation electrode. (**C**) Representative images of body surface electrocardiogram (ECG).

Hematoxylin and eosin (H&E) staining

Atrial tissue samples were fixed by immersing them in a 4% paraformaldehyde solution for subsequent detailed histological examination. Subsequently, these tissue samples were embedded in paraffin to obtain solid tissue blocks suitable for sectioning. Using a microtome, the tissue blocks were sectioned into 5 μm tissue sections. The sections were subjected to H&E staining, beginning with xylene for deparaffinization, followed by ethanol rehydration through a graded series of alcohol solutions, hematoxylin staining for 20 min to stain the cell nuclei, a brief differentiation step for 2 s, a 5-min blueing period, and eosin staining for 2 min to provide contrast to the cell cytoplasm. Finally, the HE stained sections were dehydrated with a series of alcohol solutions, naturally dried, sealed with neutral gum, and histopathological features were observed under a microscope.

Masson staining

Masson staining was used to evaluate atrial tissue fibrosis. The procedure involved staining first with Weigert iron hematoxylin for 10 min, followed by a 15 s differentiation to accentuate tissue contrast. Then, a bluing solution was applied for 3 min to enhance the staining effect. Subsequently, the slides were gently washed in a weak acid solution for 1 min to prepare for the next step. Ponceau magenta was then used for a 10 min staining to visualize the collagen fibers. The final step involved staining with toluidine blue for 2 min, which aids in distinguishing muscle from fibrous tissue. This comprehensive staining procedure allowed a clear visualization of the fibrotic changes within the atrial tissue.

Immunohistochemical staining

Paraffin blocks of atrial tissue sections were deparaffinized in xylene, hydrated with alcohol, immersed in 3% H_2O_2 for 15 min, and washed with phosphate-buffered saline (PBS). Antigen retrieval was performed using 0.1 M sodium citrate solution. The atrial tissue sections were blocked with goat serum for 1 h at room temperature (RT) and separately incubated with rabbit anti-α-SMA, p-AMPK, AMPK antibodies (1:300) overnight at 4 °C, and subsequently with goat anti-rabbit HRP

conjugated secondary antibody (1:300) at room temperature for 1 h. Hematoxylin was added to stain nuclei and incubated for 15 min. α-SMA positive expression was observed under a microscope.

Transcriptome sequencing and analysis

Trizol reagent was used to extract total RNA from rabbit atrial tissue in the RAP and RAP + BBR groups, and three samples from each group were randomly selected for sequencing analysis. The concentration and quality of extracted RNA were determined using a NanoDrop 2000 ultraviolet spectrophotometer (Thermo Fisher Scientific Inc., Waltham, MA, USA) and an Agilent 2100 bioanalyzer (Agilent Technologies Inc., Santa Clara, CA, USA), and the qualified RNA was used for cDNA synthesis. The cDNA library was sequenced using the Illumina HiSeq 4000 sequencing system (Illumina, San Diego, CA, USA). Bioinformatics analysis was performed using the Boao Crystal platform. The differentially expressed genes (DEGs) were screened using the DESeq2 package (Bioconductor, version 3.14), with the following screening criteria: Fold Change >1.5 and FDR <0.05. The DEGs were analyzed using the DAVID 6.8 database (https://david.ncifcrf.gov/) for the Kyoto Encyclopedia of Genes and Genomes (KEGG) enrichment analysis, and Cytoscape for their protein-protein interaction network and co-expression analysis. The threshold of significant enrichment was $P < 0.05$.

Quantitative real time polymerase chain reaction (qPCR)

Total RNA was isolated from heart tissue using an RNA extraction kit. cDNA was synthesized using the extracted RNA as a template, and the reverse transcription reaction system was prepared according to the formula specified in the Evo M-MLV reverse transcription Premix kit (Accurate Biotechnology Co., Ltd.). Subsequently, quantitative real time polymerase chain reaction (qPCR) analysis was performed using the SYBR Green Pro Taq HS Premix qPCR Kit (Accurate Biotechnology Co., Ltd.). The expression genes were normalized to the expression of ACTB and calculated using the $2^{-\Delta\Delta Ct}$ method. The sequences of primers used are shown in Table 1.

Table 1. Primer sequences

Gene	Primer name	Sequence (5' to 3')	Product size
AMPK	FORWARD	GTGAGCAAGCCGTGTACTGTG	101
	REVERSE	AGCAGGTCGTCCATGAGGTTC	101
PPARα	FORWARD	GAGTGTTCGGAGGAGGAGGTC	92
	REVERSE	CTGTTGTCTATGATGAGGTGGTAGG	92
β-actin	FORWARD	AGAAGGTGGTGAAGCAGGCATC	111
	REVERSE	CGAAGGTGGAAGAGTGGGAGTTG	111

Western blot

Western blot analysis was performed as previously described. Briefly, total atrial tissue protein was extracted, and the protein concentration was determined using the bicinchoninic acid (BCA) protein concentration assay kit and adjusted for consistency. The denatured protein sample (20 μg) was separated by sodium dodecyl sulfate polyacrylamide gel electrophoresis (SDS-PAGE) and transferred to polyvinylidene fluoride membranes (Bio-Rad Laboratories, Hercules, CA, USA). After blocking the membranes with 5% buttermilk, the membranes were incubated at 4 °C overnight separately with ACTB, α-SMA, PPARα, p-AMPK, and AMPK antibodies (dilution 1:2,000). Subsequently, after washing three times with Tris-buffered saline with Tween 20 (TBST) solution, membranes were incubated with HRP-labelled secondary antibody (dilution 1:2,000) at room temperature for 1 h. We performed a semi-quantitative analysis of the immunoreactive protein bands by densitometry using the ImageJ analysis software [National Institute of Health (NIH), Bethesda, MD, USA]. The relative protein expression was calculated as the relative ratio of the densitometric value of the target protein to the densitometric value of ACTB.

Molecular docking

We used the computerized protein ligand docking software Autodock Vina 1.2.2 (https://rsd3.scripps.edu/) to evaluate the binding energy and interaction pattern between BBR and the targets AMPK and PPARα. First, the two-dimensional structure of BBR was obtained from PubChem and PDB database (https://www.rcsb.org/), and the protein and ligand files were preliminarily prepared. All protein and molecular files were converted to PDBQT format, removing all water molecules and adding polar hydrogen atoms. To facilitate the movement of free molecules, we set the grid framework so that its central location contains each protein domain. The binding bag is defined as a cube area of dimensions 30Å × 30Å × 30Å with a grid spacing of 0.05 nm. Then, we used Autodock Vina 1.2.2 molecular docking software (http://autodock.scripps.edu/) to complete the modeling and for visualization.

Molecular dynamics (MD) simulations

We performed molecular dynamics (MD) simulations using the Amber and AmberTools software package to evaluate the stability of the selected docking model (Sharma et al., 2022; Sun et al., 2023). Proteins use ff14SB force fields in the TIP3P water model, while small molecules use GAFF force fields. The ligands were prepared by the Antechamber module, and the proteins were pretreated by the Tleap module. After minimizing the system energy, the temperature gradually increased from 0 K to 300 K over a period of 30 ps. Then, using NVT and NPT integration, the system reached equilibrium at 300 K. MD simulations lasting 100 ns were performed under periodic boundary conditions of constant temperature and pressure. The root mean square deviation (RMSD) of the MD trajectory was calculated, and the results were visualized using the Xmgrace program and Visual Molecular Dynamics (VMD). Combined with the free energy, the molecular mechanics generalized Born surface area (MM/GBSA) method, and the molecular mechanics Poisson–Boltzmann surface area (MM/PBSA) method were used to calculate the results.

Statistical analysis

Statistical analyses were performed using the GraphPad Prism (version 9.0) software (GraphPad Software Inc., San Diego, CA, USA). Data are presented as the mean ± SD (standard deviation). To determine the significance of differences across multiple groups, a one-way analysis of variance (ANOVA) test was used, complemented by either Bonferroni's *post hoc* test or Dunnett's multiple comparison test, as specified in the analysis. When the comparison was limited to two groups, an independent Student's *t*-test was used. Statistical significance was defined as a P value of less than 0.05.

Results

Effect of BBR on LAW/BW and myocardial pathological injury

In the model of AF, the increased ratio of atria to body weight (BW) is considered an important feature of atrial remodeling (Lavie et al., 2017). Our results revealed that the ratio of left atrial weight (LAW) to BW in the RAP group was significantly higher than that in the control group, while LAW/BW was significantly lower after BBR intervention (Fig. 2A). To exclude the influence of the BW of the rabbit, the BW and LAW were determined individually in each group, and the results showed that there was no significant difference in BW among all groups (Fig. 2B). The variation trend of the LAW was consistent with the LAW/BW (Fig. 2C). Thus it was assumed that the difference in the LAW/BW among all groups was due to the change of the LAW, and BBR could significantly reduce atrial enlargement caused by AF. Histopathological examination of the injury of myocardial tissue in each group by H&E staining revealed neatly and densely arranged myocardial fibers, with clear nuclei, and reduced ECM in the control group, while in the RAP group, the myocardial fibers were atrophied, disordered, and infiltrated by many inflammatory cells. In addition, compared with the RAP group, the above histopathological changes were significantly reduced in the RAP + BBR group. The pathological changes in the sham group and sham + BBR group were similar (Fig. 2D).

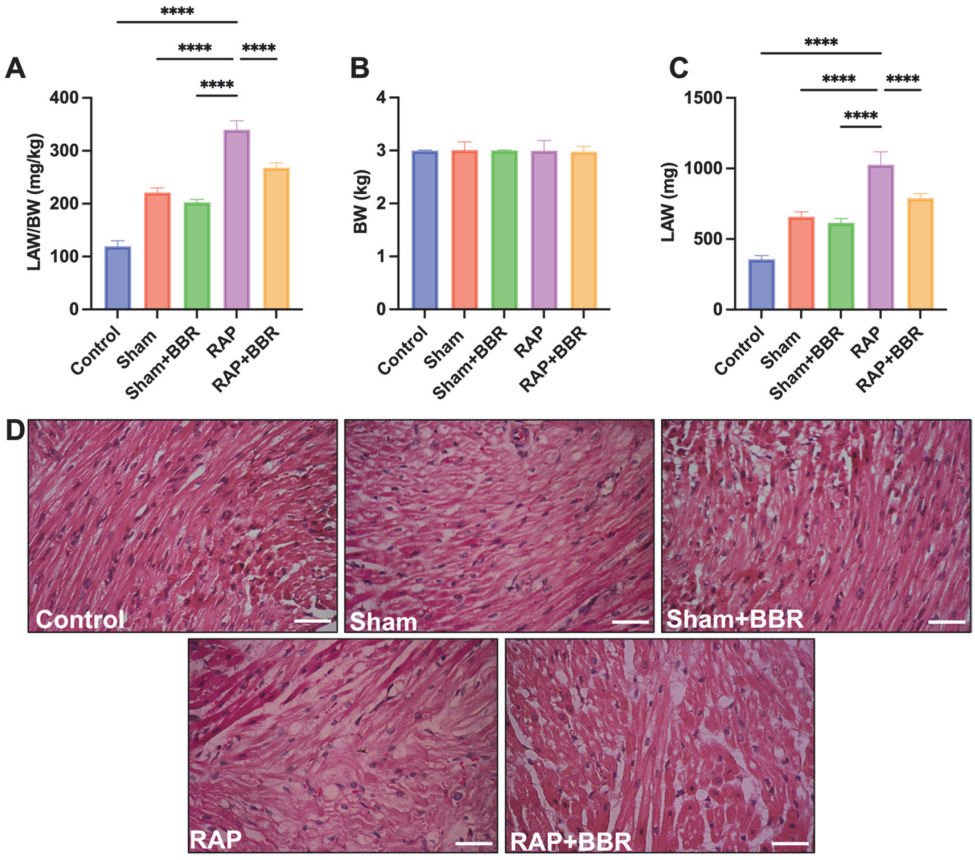

Fig. 2. Effect of BBR on LAW/BW and myocardial pathological injury. (**A**) Statistical analysis of the ratio of left atrial weight to body weight of rabbits in each group (mg/kg) (n = 6). (**B**) Statistical analysis chart of body weight of rabbits in each group (kg) (n = 6). (**C**) Statistical analysis of left atrial weight of rabbits in each group (mg) (n = 6). (**D**) Representative images of HE staining of heart tissue sections (n = 6), Scale bar = 50 μm. All data are presented as the mean ± SD, **** P < 0.0001.

Effect of BBR on myocardial fibrosis in rabbits

To evaluate the effect of BBR on myocardial fibrosis in RAP rabbits, we initially used Masson staining to examine the levels of fibrosis (Liu et al., 2023a). The results revealed that myocardial fibers in the control group were neatly arranged, with normal nucleus size and no blue collagen deposition, indicating the absence of fibrosis. In contrast, a similar small amount of collagen deposition was observed in the myocytes of rabbits in the sham and sham + BBR groups, and in the RAP group the area of myocardial fibrosis increased. But it was significantly decreased in the RAP + BBR group compared to the RAP group (Fig. 3A). Additionally, quantitative analysis of the collagen volume fraction (CVF) in the atrial tissue of rabbits across the groups revealed a significant increase in myocardial interstitial fibrosis in the RAP group compared to the control group (P < 0.001), while the collagen fiber area in the RAP + BBR group was significantly reduced compared to the RAP group (P < 0.001). The degree of collagen fiber deposition in the sham and sham + BBR groups was comparable to that in the control group, but significantly lower than that in the RAP group (Fig. 3B, P < 0.05). Further evaluation of the effect of BBR on the expression of α-SMA by immunohistochemical staining revealed varying degrees of brown or yellow spots in atrial myocytes, indicating positive immunohistochemical staining for α-SMA across all groups. Only minimal positive staining for α-SMA was observed in the control group, sham and sham

+ BBR groups, whereas pronounced positive expression was found in the RAP group, where the cytoplasm appeared brownish yellow, but cytoplasmic staining was significantly reduced in the RAP + BBR group compared to the RAP group (Fig. 3C). Western blot analysis further confirmed the inhibitory effect of BBR on α-SMA expression, revealing that the α-SMA expression level in the RAP + BBR group was significantly lower than that in the RAP group (Fig. 3D–E). These findings suggest that BBR can reduce myocardial fibrosis in RAP rabbits.

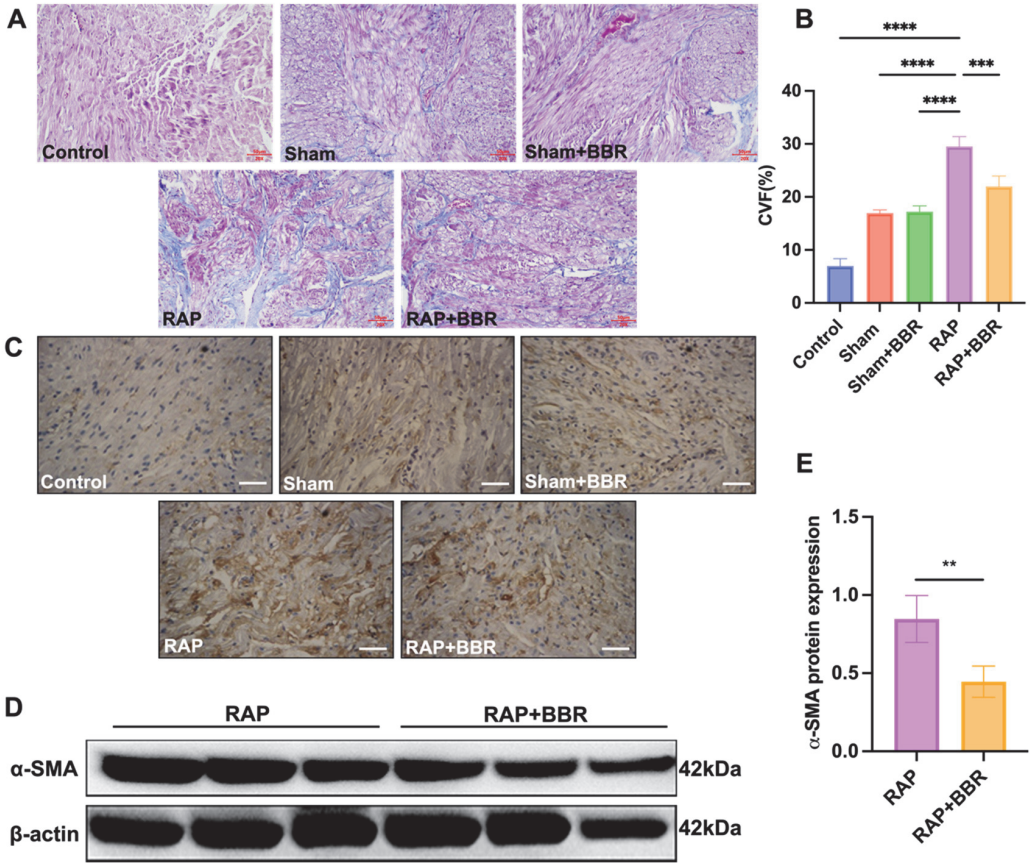

Fig. 3. Effect of BBR on myocardial fibrosis in rabbits. (**A**) Representative images of Masson staining of rabbit heart tissue in each group (n = 6). (**B**) Statistical analysis diagram of collagen volume fraction (CVF) of rabbits in each group (n = 6). (**C**) Representative images of immunohistochemical staining of α-SMA protein expression in rabbit heart tissue in each group (n = 6). (**D**) Representative image of Western blot immunoreactive band of α-SMA protein in the RAP and RAP + BBR groups (n = 3). (**E**) Statistical analysis of α-SMA protein expression levels (n = 3). All data are presented as the mean ± SD, ** P < 0.01, **** P < 0.0001, Scale bar = 50 μm.

Effects of BBR on oxidative stress and inflammation of the myocardium

Growing research indicates that oxidative stress and inflammation play significant roles in the development of AF (Karam et al., 2017). On the one hand, oxidative stress and inflammation contribute to both electrical and structural remodeling of the atrium, which can lead to the onset of AF (Balan et al., 2024). On the other hand, AF itself can exacerbate atrial remodeling and the inflammatory response, thereby contributing to the persistence of the condition (Ramos-Mondragón et al., 2023). Therefore, anti-inflammatory and antioxidant therapies may represent novel strategies for the treatment of AF. The results of this study revealed that, compared to the control, sham, and sham + BBR groups, the SOD activity of the serum of rabbits in the RAP group was significantly reduced, while the MDA content was significantly increased. Additionally, the expression levels of IL-1β, IL-6, and TNF-α were significantly elevated in the RAP group. In contrast, the serum SOD activity in the RAP + BBR group was significantly increased, the MDA content was significantly decreased, and the expression levels of the inflammatory cytokines IL-1β, IL-6, and TNF-α were significantly reduced (Fig. 4). These findings suggest that BBR may inhibit oxidative stress and inflammatory responses, thereby mitigating atrial electrical remodeling.

Transcriptomic analysis of BBR-regulated atrial remodeling in RAP rabbits

To analyze the potential mechanism by which BBR improves atrial remodeling in rabbits with right atrial pressure, transcriptome sequencing was performed on the heart tissues of rabbits from both the RAP and RAP + BBR groups. The results, shown in Fig. 5A, indicate that the gene expression abundance in all samples met the necessary criteria. Additionally, the Pearson correlation coefficient showed a strong correlation between the two sample groups, revealing significant differences in genetic profiles between the RAP and RAP + BBR groups (Fig. 5B). The volcano plot of differentially expressed genes (DEGs) in the RAP and RAP + BBR groups is shown in Fig. 5C. Compared to the RAP group, a total of 376 DEGs were identified in the RAP + BBR group, comprising 228 upregulated

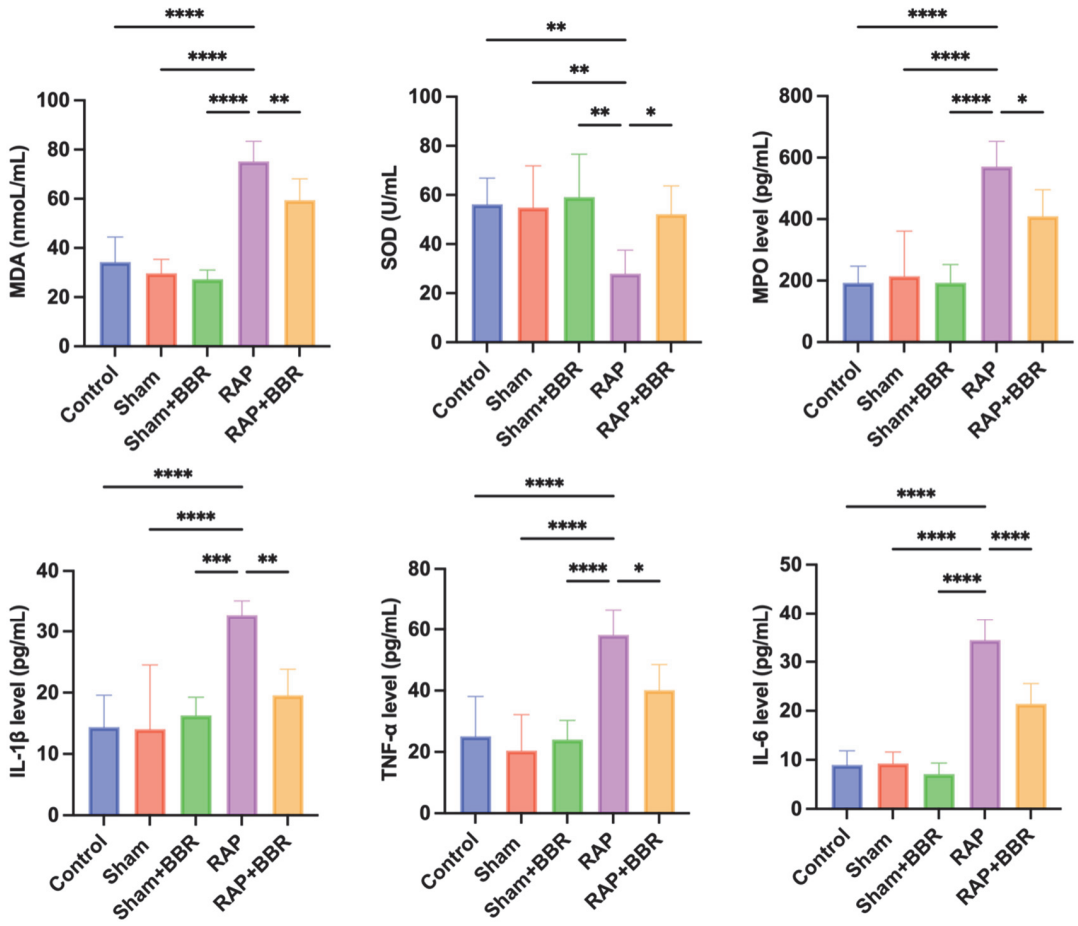

Fig. 4. Effects of BBR on oxidative stress and inflammation of myocardium. Quantitative statistical analysis results of SOD activity, MDA content, and expression levels of IL-1β, IL-6, and TNF-α in serum of rabbits from each group (n = 6). All data are presented as the mean ± SD, * P < 0.05, ** P < 0.01, *** P < 0.001, **** P < 0.0001.

DEGs and 148 downregulated DEGs. The expression pattern clusters of these significant DEGs are depicted as a heatmap in Fig. 5D. To further elucidate the underlying biological processes, Gene Ontology (GO) term enrichment analysis was performed on the DEGs in the RAP and RAP + BBR groups. The GO term enrichment analysis revealed that the biological processes primarily associated with these DEGs are cellular processes, signal transduction, and biological regulation. Cellular components mainly include cells, cell parts, and cell membranes, while molecular functions largely comprise binding, catalytic activity, and molecular transduction activity (Fig. 5E). In addition, KEGG pathway enrichment analysis to identify cell signaling pathways related to these DEGs between the RAP and RAP + BBR groups (Fig. 5F–G) identified the PPARα signaling pathway, adipocytokine signaling pathway, ECM-receptor interaction, longevity-regulating pathway, and AMPK signaling pathway, among others. Notably, our results suggest that the PPAR and AMPK signaling pathways play a crucial role in regulating atrial remodeling in the RAP group rabbits. Previous studies have indicated that the PPARα and AMPK pathways can influence the atrial remodeling process in a RAP-induced AF rabbit model by regulating energy metabolism, providing myocardial protection, exerting anti-inflammatory and antioxidant effects, and modulating autophagy. Thus, these pathways significantly impact the occurrence and progression of AF.

Effects of BBR on the expression of genes and proteins associated with the AMPK/PPARα pathway

Based on transcriptome analysis, the AMPK/PPARα signaling pathway warrants further investigation. We validated the transcriptomic findings using qPCR analysis and found that, compared to the RAP group, the mRNA expression levels of PPARα and AMPK in the myocardial tissue of mice from the RAP + BBR group were significantly increased (Fig. 6A–B). We also examined whether similar differential expression trends were observed at the protein level. Our results indicated that, relative to the RAP group, the protein expression levels of PPARα and p-AMPK in the myocardial tissue of the RAP + BBR group were significantly elevated (Fig. 6C–E), while the protein expression levels of AMPK did not differ significantly between the two groups (Fig. 6F, P > 0.05). These findings suggest that BBR may enhance atrial remodeling in RAP rabbits by activating the AMPK/ PPARα signaling pathway.

Molecular docking predicted the binding patterns of BBR to AMPK and PPARα

Based on transcriptomic results, we sought to investigate the significance of AMPK and PPARα signaling in the development of right atrial pressure and the therapeutic effects of BBR on AF. To further explore the role of BBR in AMPK and PPARα signaling, we performed molecular docking analyses. The binding

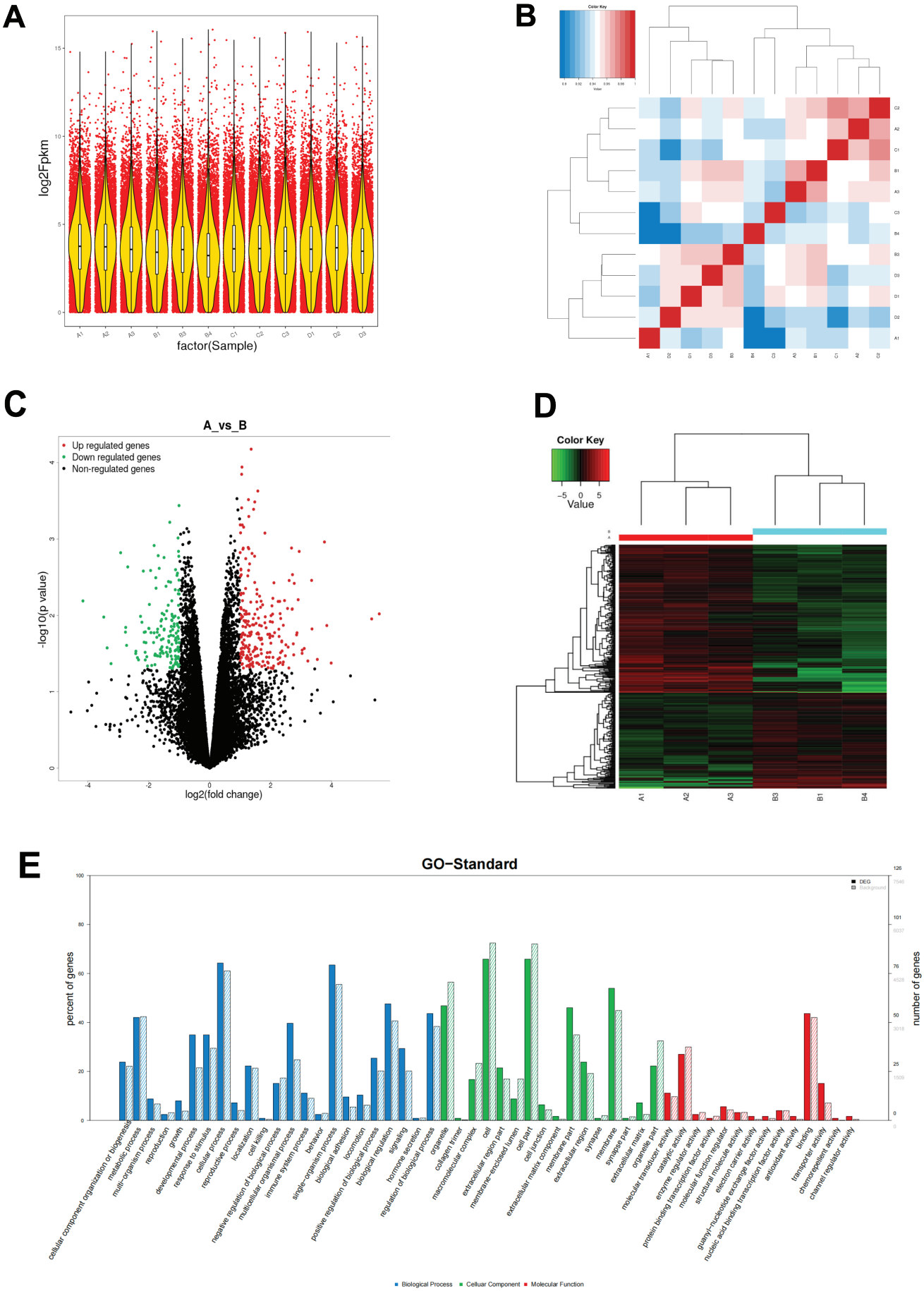
A
log2Fpkm
factor(Sample)
B
Color Key
C
A_vs_B
Up regulated genes
Down regulated genes
Non-regulated genes
-log10(p value)
log2(fold change)
D
Color Key
Value
A1
A2
A3
B3
B1
B4
E
GO−Standard
percent of genes
number of genes
DEG
Biological Process
Cellular Component
Molecular Function

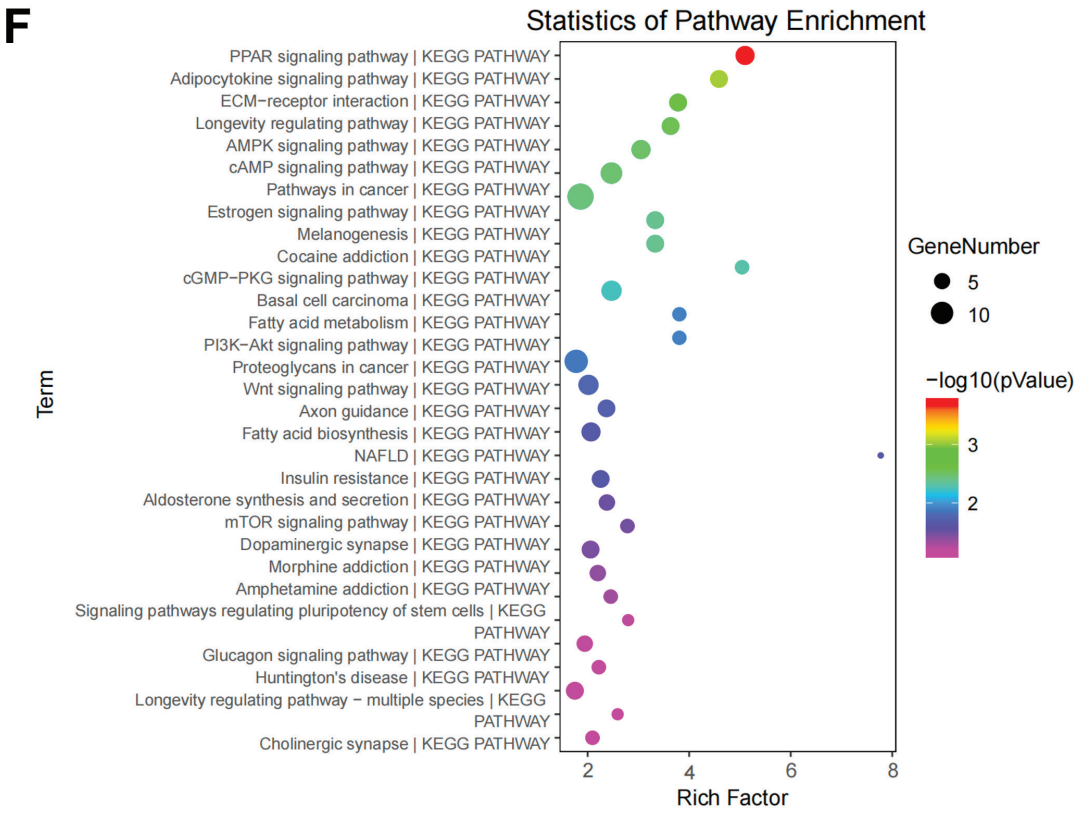

Fig. 5. Transcriptomic analysis of atrial remodeling in RAP rabbits regulated by BBR. (**A**) Violin map of gene expression levels. (**B**) Principal Component Analysis (PCA) diagram. (**C**) Gene volcano plots showing significant differences between the RAP group and the RAP + BBR group, with green circles indicating downregulated gene expression and red circles indicating upregulated gene expression. (**D**) Heatmap of significantly differentially expressed genes (DEGs) in the heart tissue of RAP group and RAP + BBR group rabbits, with darker green indicating lower expression level; the darker the red, the higher the expression level. (**E**) Histogram of gene ontology (GO) function annotation of significantly DEGs between the RAP group and RAP + BBR group. (**F**) Bubble map, showing the functional enrichment of GO with significantly DEGs in the RAP group and RAP + BBR group; (**G**) Enrichment histogram of KEGG pathways with significantly DEGs between the RAP group and RAP + BBR group.

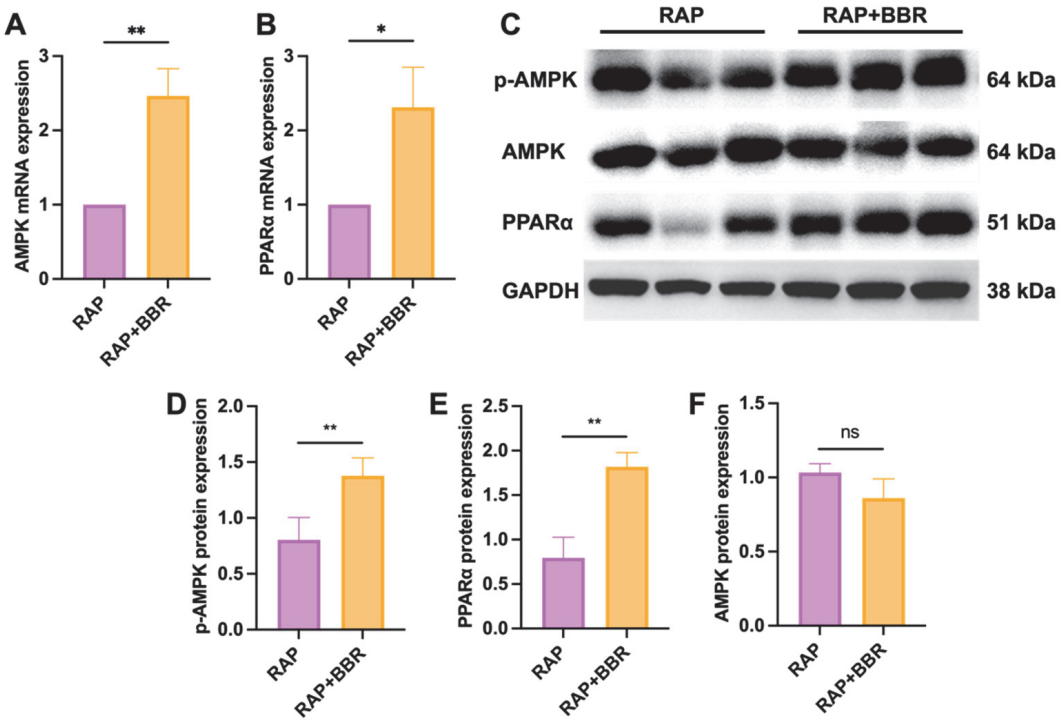

Fig. 6. Effects of BBR on the expression of genes and proteins associated with the AMPK/PPARα signaling pathway. (**A**) Semi-quantitative analysis of AMPK mRNA expression in cardiac tissue of RAP group and RAP + BBR group rabbits (n = 3). (**B**) Semi-quantitative analysis of PPARα mRNA expression in cardiac tissue of RAP group and RAP + BBR group rabbits (n = 3). (**C**) Representative strip map of key proteins of the AMPK-PPARα signaling pathway (n = 3). (**D**) Semi-quantitative analysis of the p-AMPK protein expression levels (n = 3). (**E**) Semi-quantitative analysis of PPARα protein expression levels (n = 3). (**F**) Semi-quantitative analysis of AMPK protein expression levels (n = 3). All data are presented as the mean ± SD, * P < 0.05, ** P < 0.01.

energy of the AMPK-BBR complex is –8.335 kcal/mol, while the binding energy of the PPARα-BBR complex is –8.602 kcal/mol. Both energy values are lower than –7 kcal/mol, indicating a high affinity of BBR for AMPK and PPARα, suggesting that these proteins may serve as potential targets for BBR. The AMPK protein and BBR molecules form hydrogen bonds, C-H bonds, electrostatic interactions (π-anion), hydrophobic interactions (π-sigma, amide-π stacked, alkylation, π-alkylation), and van der Waals interactions (Fig. 7A). Similarly, the PPARα protein and BBR molecules establish C-H bonds, hydrophobic interactions (π-sigma, alkylation, π-alkylation), and van der Waals interactions (Fig. 7B).

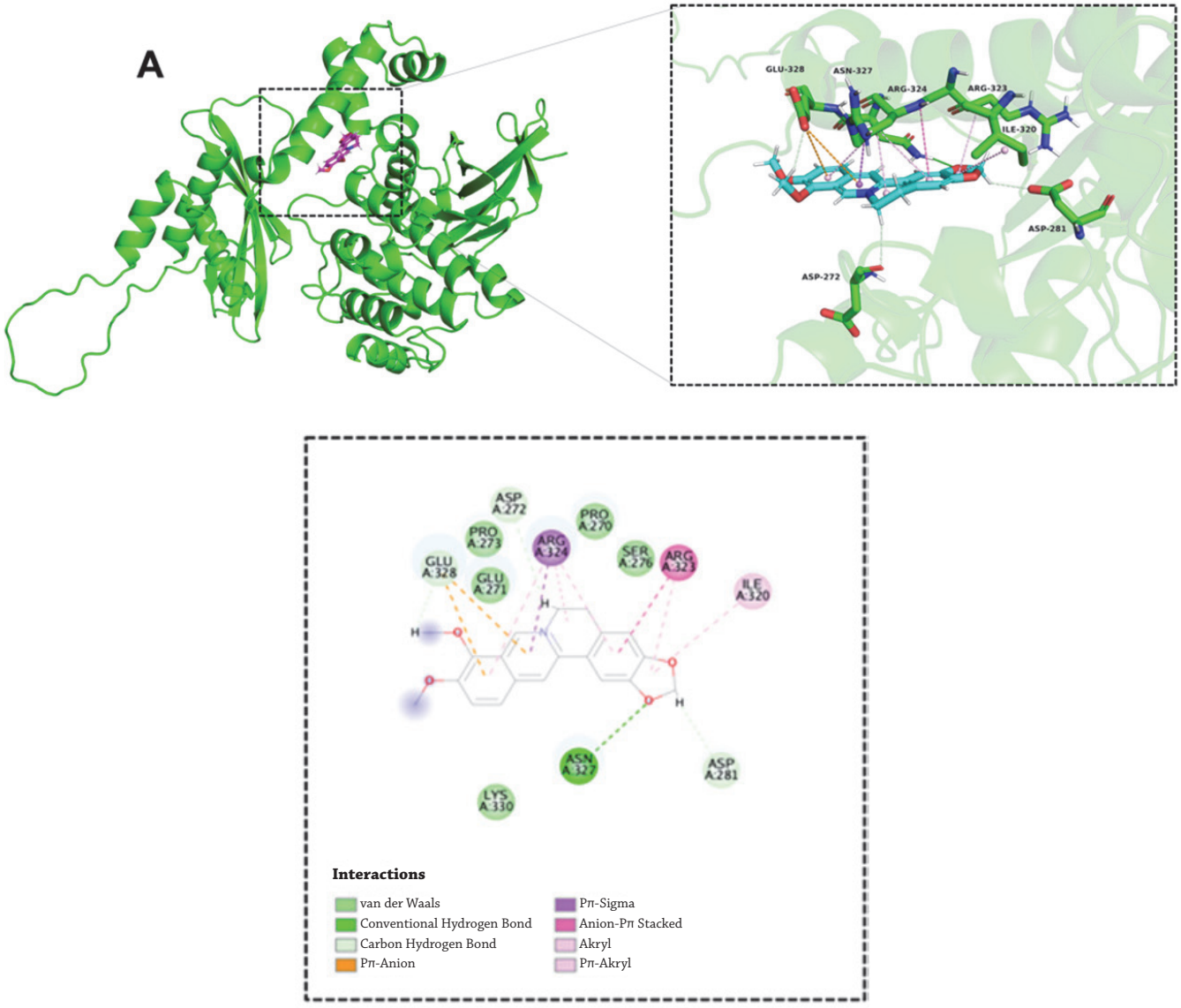

Fig. 7. Molecular docking predicted the binding patterns of BBR to AMPK and PPARα. (**A**) Two-dimensional (2D) and three-dimensional (3D) interaction diagrams of BBR and AMPK protein.

Molecular dynamics (MD) simulations verify the combination pattern of BBR with AMPK and PPARα

We investigated the stability and dynamic interactions of the AMPK-BBR and PPARα-BBR complexes by MD simulations to validate the findings from molecular docking and analyze the molecular motion of AMPK and PPARα following ligand binding. The simulations were performed over a period of 100 ns, during which the RMSD curve of the AMPK-BBR complex reached a value of 1.18 (Fig. 8A). Solvent accessible surface area (SASA) analysis revealed that the SASA curve for the AMPK-BBR complex remained relatively stable throughout the simulation period, with an initial SASA value of about 321.441 nm^2 and 264.469 nm^2 at the end of the simulation (Fig. 8B). In addition, the radius of gyration (Rg) curve for the AMPK-BBR complex also exhibited stability, with an average Rg value of 2.54 nm (Fig. 8C). Root-mean-square fluctuation (RMSF) analysis revealed that the RMSF of the AMPK-BBR complex was approximately 1.40 nm, suggesting stable protein binding to the ligand (Fig. 8D). Additionally, hydrogen bond analysis indicated that the number of hydrogen bonds within the AMPK-BBR complex fluctuated between 1 and 4 throughout the 100 ns simulation period (Fig. 8E). The binding free energy of the AMPK protein and BBR at various frames is shown in Fig. 8F, with an average binding free energy of –33.82 kcal/mol. Gibbs free energy was calculated based on the RMSD and Rg values of the AMPK-BBR complex, and both two-dimensional (2D) and three-dimensional (3D) topographies of Gibbs free energy were generated using the RMSD, Rg, and Gibbs free energy data. As shown in Fig. 8G and 8H, the Gibbs free energy diagram for the AMPK-BBR complex reveals two distinct and pronounced lowest energy regions. Additionally, the energy contributions of individual residues to the binding free energy of AMPK and BBR are shown in Fig. 8I, highlighting the amino acid residues GLU-271 and ARG-324 as significant contributors, with energy contribution values of –2.14 and –2.97 kcal/mol, respectively.

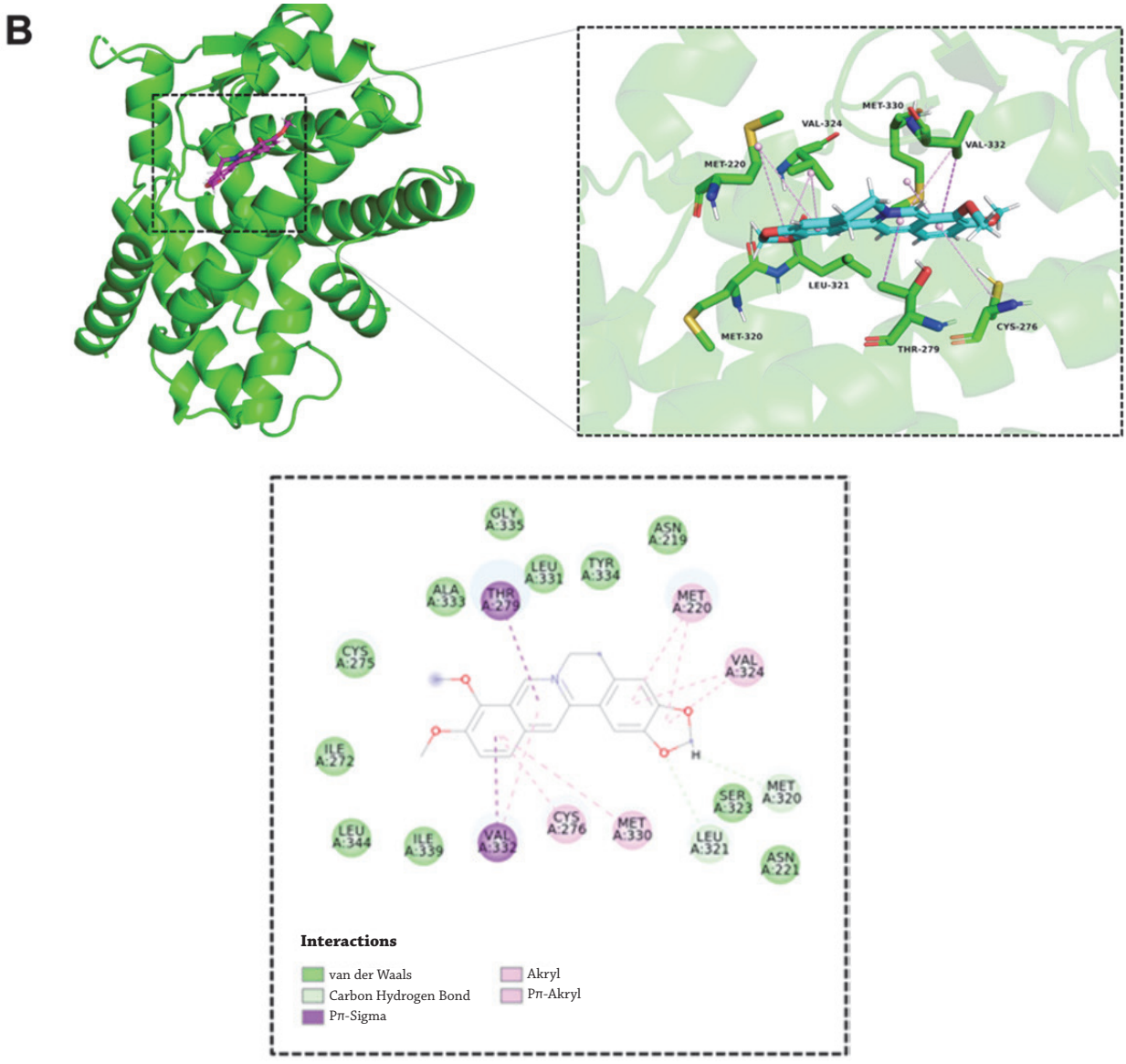

Fig. 7. Molecular docking predicted the binding patterns of BBR to AMPK and PPARα. (**B**) 2D and 3D interaction diagrams of BBR and PPARα protein.

The results of the MD simulations for the PPARα-BBR complex are shown in Fig. 9. The RMSD curve for the PPARα-BBR complex over time reached a value of 0.31 (Fig. 9A). SASA analysis revealed that the SASA value for the PPARα-BBR complex was about 131.353 nm^2 at the beginning and 132.136 nm^2 at the end of the simulation (Fig. 9B), indicating relative stability throughout the process. The Rg curve for the PPARα-BBR complex also exhibited consistent behavior during the simulation, with an average Rg value of 1.87 nm (Fig. 9C). RMSF analysis revealed that the RMSF for the PPARα-BBR complex remained below 0.70 nm throughout the simulation, suggesting that the complex maintained relative stability in binding (Fig. 9D). During the 100 ns simulation, the number of hydrogen bonds formed in the PPARα-BBR complex ranged from 1 to 2 (Fig. 9E). The binding free energy results for various frames of the PPARα protein and BBR are shown in Fig. 9F, with an average binding free energy of –49.40 kcal/mol. The Gibbs free energy diagrams of the PPAR-BBR complex, shown in Fig. 9G and 9H, reveal two distinct and pronounced lowest energy regions. In addition, the energy contributions of each residue to the binding free energy of PPARα and BBR are shown in Fig. 9I, highlighting the amino acid residues CYS-275, THR-279, LEU-321, and MET-330 as significant contributors, with energy contribution values of –1.71, –2.45, –2.47, and –1.87 kcal/mol, respectively. Thus, these findings suggest that BBR may form a stable binding interaction with both AMPK and PPARα.

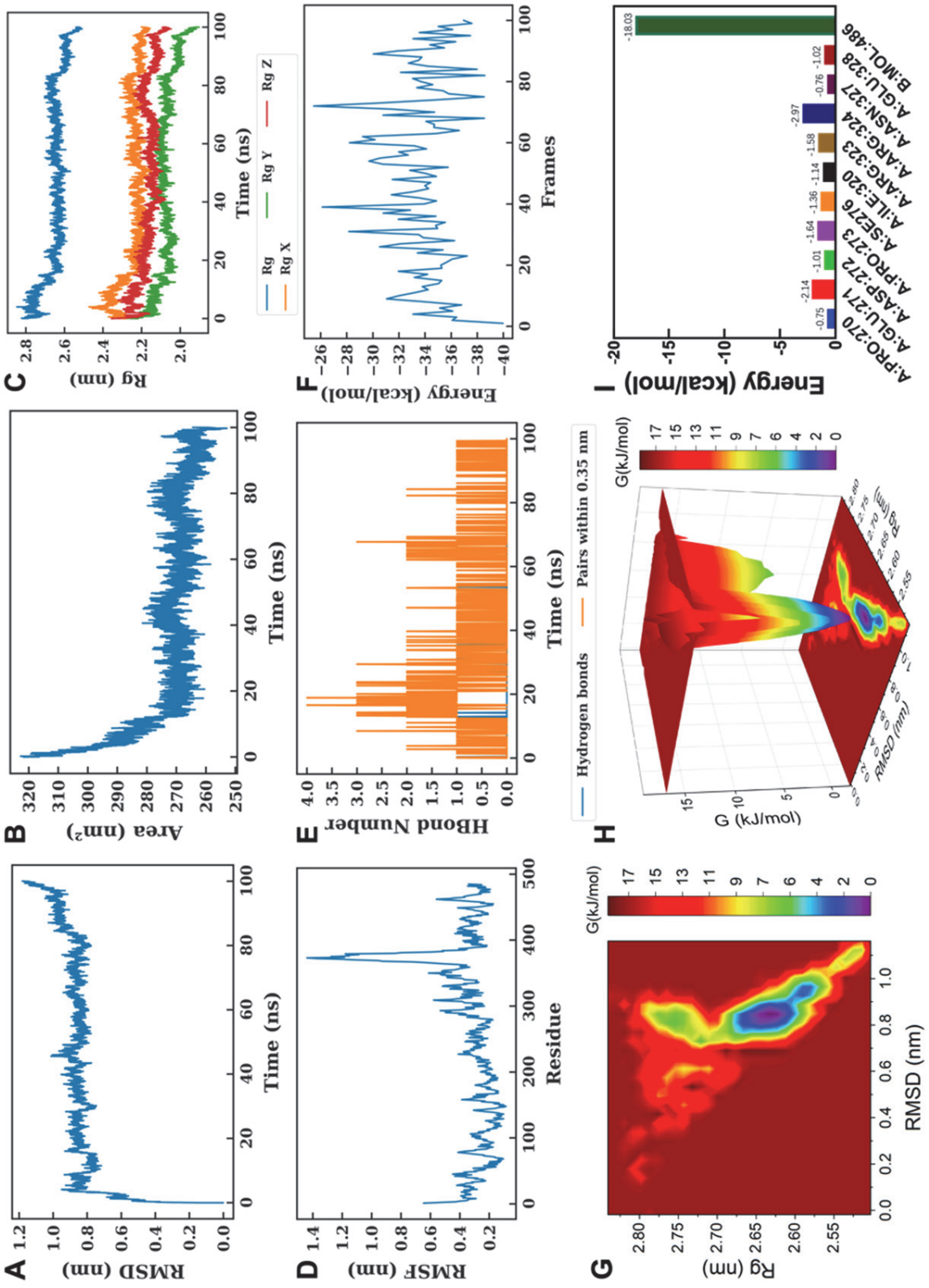

Fig. 8. MD simulations verify the binding pattern of BBR with AMPK. (**A**) RMSD curve of the AMPK protein and BBR molecule with time. (**B**) SASA curves of the AMPK protein at different times. (**C**) Rg change curve of the AMPK protein at different times. (**D**) RMSF curves of different residues of the AMPK protein. (**E**) The number of hydrogen bonds between the AMPK protein and BBR changed over time. (**F**) The binding free energy of the AMPK protein and BBR molecule at different frames. (**G**) 2D map of Gibbs free energy of the AMPK protein. (**H**) 3D map of Gibbs free energy of the AMPK protein. (**I**) Energy contribution of residues of BBR to the binding free energy of the AMPK protein.

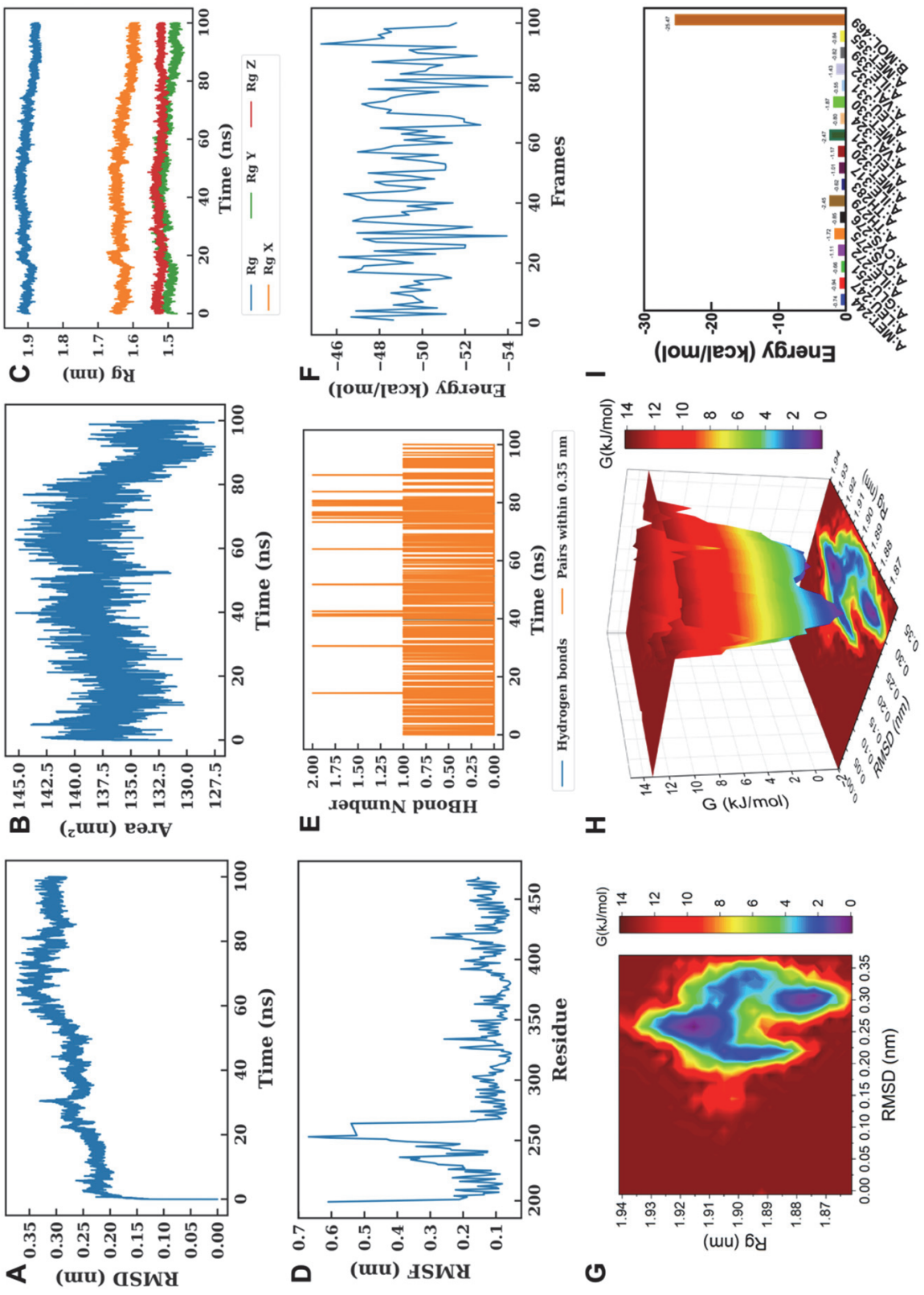

Fig. 9. MDs verifies the combination pattern of BBR with PPARα. (**A**) RMSD curve of the PPARα protein and BBR molecule over time. (**B**) SASA curves of the PPARα protein at different times. (**C**) Rg change curve of the PPARα protein at different times. (**D**) RMSF curves of different residues of the PPARα protein. (**E**) The number of hydrogen bonds between the PPARα protein and BBR changed over time. (**F**) The binding free energy of the PPARα protein and BBR molecule at different frames. (**G**) 2D map of Gibbs free energy of the PPARα protein. (**H**) 3D map of Gibbs free energy of the PPARα protein. (**I**) Energy contribution of residues of BBR to the binding free energy of the PPARα protein.

Discussion

AF is the most common arrhythmia encountered in clinical practice and is associated with significant complications, including heart failure and stroke, which can result in increased mortality. This condition profoundly impacts the longevity and quality of life of patients, while also increasing medical costs and societal burdens (Sagris et al., 2021). Currently, there is no specific pharmacological treatment for AF in clinical practice. To date, traditional anti-arrhythmic drugs have not achieved the desired efficacy, and the incidence of adverse drug reactions is substantial (Pedro et al., 2020). Therefore, the discovery of new anti-AF treatments is urgently needed. Traditional Chinese medicine, with its extensive history, has played a significant role in the clinical management of cardiovascular diseases (Dong et al., 2017; Wang et al., 2017b). Actively researching and developing the application of traditional Chinese medicine in the treatment of AF represents a novel approach to managing this condition. Studies have indicated that BBR has myocardial protective effects against arrhythmias and heart failure (An et al., 2022; Yang, et al., 2022). Furthermore, our preliminary findings suggest that BBR has a significant therapeutic effect in the treatment of AF. Our results indicate that BBR can reduce myocardial fibrosis, thereby decreasing the incidence of AF, and may provide a new therapeutic strategy for addressing both myocardial fibrosis and AF.

Atrial remodeling is a critical factor in the development of AF, with atrial enlargement and myocardial fibrosis being its primary features. This process is irreversible, making the delay of myocardial fibrosis a potential strategy for the treatment and prevention of AF (Nattel, 2017). As a result, it has emerged as an attractive treatment target and a focal point in recent research on AF prevention and management. Our results indicate that BBR significantly reduces the ratio of LAW to BW (LAW/BW), suggesting an improvement in atrial enlargement in RAP rabbits. The activation of myocardial fibroblast transdifferentiation and the subsequent excessive deposition of myocardial interstitial collagen are key cellular events that drive the fibrotic response during cardiac stress, representing important features of myocardial fibrosis (Lv et al., 2020). The myocardial CVF in atrial tissue serves as an index of the clinical degree of myocardial fibrosis (Wang et al., 2023). Additionally, changes in the expression level of alpha smooth muscle actin (α-SMA) are positively correlated with the severity of myocardial fibrosis (Begg et al., 2020). Our findings also revealed that collagen deposition, CAF%, and α-SMA expression levels in myocardial tissue from the RAP group were significantly increased compared to those in the control and sham groups. Following BBR intervention, these indices were significantly reduced, indicating that BBR can improve myocardial fibrosis in the RAP-induced AF rabbit model. In conclusion, our results preliminarily establish that BBR can improve the major pathological features of atrial remodeling in the RAP-induced AF rabbit model.

Oxidative stress and inflammation play significant roles in the process of atrial remodeling. Under normal physiological conditions, the body maintains a balance between oxidant and antioxidant (Yuan et al., 2022). However, in pathological states, the activation of the NADPH enzyme leads to the production of excessive reactive oxygen species (ROS), resulting in an imbalance between oxidative and antioxidative effects (Zhao et al., 2023). Elevated levels of ROS directly contribute to myocardial cell damage and necrosis, while also promoting the activation of fibroblasts and the progression of fibrosis (Jalife and Kaur, 2015). SOD is a crucial component of the antioxidant enzyme system, whereas MDA is a byproduct of lipid peroxidation induced by free radicals, providing a direct measure of ROS content in the body. Increased MDA levels can reduce the excitability of cardiomyocytes and prolong the duration of the action potential, thereby facilitating the onset of AF (Fu et al., 2015). In the model of AF, a significant decrease in serum SOD activity is observed, alongside a notable increase in MDA levels. This indicates an imbalance between oxidative and antioxidative processes (Liu et al., 2014). MPO, a heme protease secreted by activated neutrophils and monocytes, is closely associated with various cardiovascular diseases and is implicated in the pathogenesis of AF. MPO catalyzes the production of multiple active substances, mediates various intracellular signaling pathways, and ultimately promotes atrial remodeling, leading to the development of AF. Similarly, inflammation plays a regulatory role in the remodeling of the myocardium. Inflammatory cytokines can induce degeneration and necrosis of cardiomyocytes, alter the electrophysiological activity of the myocardium, and promote ectopic reentry of sodium, potassium, calcium, and other ions. Inhibiting inflammation can effectively prevent myocardial remodeling, thereby reducing the frequency and duration of AF (Ali et al., 2016; Souza-Neto, et al., 2022). Other studies have demonstrated that elevated levels of inflammatory cytokines, such as IL-1β, IL-6, and TNF-α, correlate with the degree of atrial enlargement, indicating that inflammation is involved in the onset and progression of AF (Hanna and Frangogiannis, 2020). In this study, BBR significantly reduced serum levels of MDA, MPO, IL-6, IL-1β, and TNF-α in rabbits, while increasing SOD activity, suggesting that its anti-AF effect may be linked to its antioxidant and anti-inflammatory properties.

AMPK is a crucial regulator of cellular energy metabolism, primarily overseeing the energy homeostasis of the heart, and is recognized as a sensor of metabolic stress. Recent studies have demonstrated that AMPK has a protective effect on atrial remodeling (Qin et al., 2024). The AMPK signaling pathway is influenced by BBR, which has long been regarded as an AMPK activator (Zhu et al., 2019). Research indicates that BBR enhances the inhibitory effect of macrophages on the production of inducible nitric oxide synthase (iNOS), cyclooxygenase-2 (COX-2), and other pro-inflammatory cytokines through AMPK activation. Upon AMPK activation, the expression of inflammatory cytokines, such as TNF-α, IL-6, NOS2, and PTGS2, is downregulated in various cell types, highlighting its significance as a key target for the anti-inflammatory activity of BBR (Li et al., 2014). PPARα is a crucial member of the PPAR family, which consists of nuclear transcription factors activated by ligands. PPARα is predominantly expressed in the liver, skeletal muscle, kidneys, heart, and the vascular wall, and plays a central role in inflammation, oxidative fatty acid catabolism, energy metabolism, immune response, and cell differentiation (Wang et al., 2024). In recent years, the role of PPARα in the inflammatory response has gained increasing attention (Gao et al., 2018). Its anti-inflammatory effects are primarily achieved by inhibiting the production of adhesion molecules, pro-inflammatory cytokines, and ECM proteins, as well as by stimulating the activity of anti-inflammatory molecules and regulating the transcriptional expression of genes associated with the inflammatory response (Gao et al., 2018). Several studies have demonstrated that PPARα serves as a crucial regulator of inflammation and myocardial fibrosis in models of AF. The activation of PPARα significantly suppresses the release of inflammatory factors, thereby mitigating the inflammatory response (Park et al., 2024; Xu et al., 2024; Zhang

et al., 2024). This study used transcriptomics to investigate the mechanism by which BBR improves atrial remodeling in a RAP-induced AF rabbit model, revealing that the mechanism of action of BBR primarily involves the AMPK-PPARα pathway. The findings by qPCR and Western blot analyses corroborated the transcriptomic results, indicating that BBR enhances the expression of AMPK and PPARα mRNA, as well as the proteins AMPK and p-PPARα in the AMPK-PPARα signaling pathway. To further ascertain whether BBR directly interacts with AMPK and PPARα to exert its regulatory effects, we performed molecular docking and MD simulations to determine their binding patterns. The results confirmed that BBR can directly target AMPK and PPARα, potentially binding to specific amino acid residues, such as GLU-271 and ARG-324 of AMPK, and CYS-275, THR-279, LEU-321, and MET-330 of PPARα. Collectively, these findings suggest that BBR may reduce oxidative stress and inflammation in the RAP-induced AF rabbit model by activating the AMPK-PPARα signaling pathway, thereby reducing myocardial fibrosis and atrial remodeling, ultimately improving AF.

Conclusion

This study demonstrates that BBR can reduce the weight of the left atrium, decrease the area of myocardial fibrosis, inhibit the expression of α-SMA protein in atrial tissue, and reduce inflammation and oxidative stress. Furthermore, BBR effectively inhibits atrial structural remodeling, thereby contributing to the prevention of AF. BBR may also activate the AMPK-PPARα signaling pathway by directly binding to AMPK and PPARα, which may further improve AF. However, the specific mechanism of action requires further research.

Consent for publication

All authors have read, revised, and approved the final manuscript.

Ethics approval and consent to participate

All procedures were performed according to the guidelines of Liaoning University of Traditional Chinese Medicine Institutional Animal Care and Use Committee. This research was approved by Liaoning University of the Traditional Chinese Medicine Institutional Animal Care and Use Committee.

Acknowledgements

We would like to acknowledge the support of the Liaoning Provincial Department of Science and Technology for this study, as well as the contributions of Liaoning University of Traditional Chinese Medicine and the General Hospital of Northern Theater Command for providing the experimental platform.

CRediT authorship contribution statement

Yang Wang: Writing – review and editing, Writing – original draft, Writing – review and editing, Funding acquisition, Project administration. *Zhe Sun:* Visualization, Methodology, Data curation. *Zong-tao Yin:* Software, Formal analysis. *Jian Zhang:* Visualization. *Fang-ran Xin:* Resources, Investigation. *Yin-li Xu:* Visualization, Supervision. *Huai Lan:* Formal analysis, Methodology.

Funding

This research was supported by the Natural Science Foundation of Liaoning Province (No. 2024-MS-251).

Declaration of competing interest

The authors declare that they have no known competing financial interests or personal relationships that could have influenced the work reported in this paper.

References

Ali M, Pulli B, Courties G, Tricot B, Sebas M, Iwamoto Y, et al. (2016). Myeloperoxidase Inhibition Improves Ventricular Function and Remodeling After Experimental Myocardial Infarction. JACC Basic Transl Sci 1(7): 633–643. DOI: 10.1016/j.jacbts.2016.09.004.

An N, Zhang G, Li Y, Yuan C, Yang F, Zhang L, et al. (2022). Promising Antioxidative Effect of Berberine in Cardiovascular Diseases. Front Pharmacol 13: 865353. DOI: 10.3389/fphar.2022.865353.

Balan AI, Halațiu VB, Scridon A (2024). Oxidative Stress, Inflammation, and Mitochondrial Dysfunction: A Link between Obesity and Atrial Fibrillation. Antioxidants (Basel) 13(1): 117. DOI: 10.3390/antiox13010117.

Begg GA, Swoboda PP, Karim R, Oesterlein T, Rhode K, Holden AV, et al. (2020). Imaging, biomarker and invasive assessment of diffuse left ventricular myocardial fibrosis in atrial fibrillation. J Cardiovasc Magn Reson 22(1): 13. DOI: 10.1186/s12968-020-0603-y.

Brenyo AJ, Aktas MK (2011). Non-pharmacologic management of atrial fibrillation. Am J Cardiol 108(2): 317–325. DOI: 10.1016/j.amjcard.2011.03.043.

Cheng D, Liu P, Wang Z (2022). Palmatine attenuates the doxorubicin-induced inflammatory response, oxidative damage and cardiomyocyte apoptosis. Int Immunopharmacol, 106: 108583. DOI: 10.1016/j.intimp.2022.108583.

Dong Y, Liao J, Yao K, Jiang W, Wang J (2017). Application of Traditional Chinese Medicine in Treatment of Atrial Fibrillation. Evid Based Complement Alternat Med 2017: 1381732. DOI: 10.1155/2017/1381732.

Feng X, Sureda A, Jafari S, Memariani Z, Tewari D, Annunziata G, et al. (2019). Berberine in Cardiovascular and Metabolic Diseases: From Mechanisms to Therapeutics. Theranostics 9(7): 1923–1951. DOI: 10.7150/thno.30787.

Fu H, Li G, Liu C, Li J, Wang X, Cheng L, Liu T (2015). Probucol prevents atrial remodeling by inhibiting oxidative stress and TNF-α/NF-κB/TGF-β signal transduction pathway in alloxan-induced diabetic rabbits. J Cardiovasc Electrophysiol 26(2): 211–222. DOI: 10.1111/jce.12540.

Gao L, Liu Y, Guo S, Xiao L, Wu L, Wang Z, et al. (2018). LAZ3 protects cardiac remodeling in diabetic cardiomyopathy via regulating miR-21/PPARa signaling. Biochim Biophys Acta Mol Basis Dis 1864(10): 3322–3338. DOI: 10.1016/j.bbadis.2018.07.019.

Gutierrez C, Blanchard DG (2016). Diagnosis and Treatment of Atrial Fibrillation. Am Fam Physician 94(6): 442–452.

Hanna A, Frangogiannis NG (2020). Inflammatory Cytokines and Chemokines as Therapeutic Targets in Heart Failure. Cardiovasc Drugs Ther 34(6): 849–863. DOI: 10.1007/s10557-020-07071-0.

Jalife J, Kaur K (2015). Atrial remodeling, fibrosis, and atrial fibrillation. Trends Cardiovasc Med 25(6): 475–484. DOI: 10.1016/j.tcm.2014.12.015.

Jia X, Shao W, Tian S (2022). Berberine alleviates myocardial ischemia-reperfusion injury by inhibiting inflammatory response and oxidative stress: the key function of miR-26b-5p-mediated PTGS2/MAPK signal transduction. Pharm Biol 60(1): 652–663. DOI: 10.1080/13880209.2022.2048029.

Karam BS, Chavez-Moreno A, Koh W, Akar JG, Akar FG (2017). Oxidative stress and inflammation as central mediators of atrial fibrillation in obesity and diabetes. Cardiovasc Diabetol 16(1): 120. DOI: 10.1186/s12933-017-0604-9.

Lavie CJ, Pandey A, Lau DH, Alpert MA, Sanders P (2017). Obesity and Atrial Fibrillation Prevalence, Pathogenesis, and Prognosis: Effects of Weight Loss and Exercise. J Am Coll Cardiol 70(16): 2022–2035. DOI: 10.1016/j.jacc.2017.09.002.

Li Z, Geng YN, Jiang JD, Kong WJ (2014). Antioxidant and anti-inflammatory activities of berberine in the treatment of diabetes mellitus. Evid Based Complement Alternat Med 2014: 289264. DOI: 10.1155/2014/289264.

Liu D, Chen H, Fu Y, Yao Y, He S, Wang Y, et al. (2023a). KCa3.1 Promotes Proinflammatory Exosome Secretion by Activating AKT/Rab27a in Atrial Myocytes during Rapid Pacing. Cardiovasc Ther 2023: 3939360. DOI: 10.1155/2023/3939360.

Liu T, Zhao H, Li J, Korantzopoulos P, Li G (2014). Rosiglitazone attenuates atrial structural remodeling and atrial fibrillation promotion in alloxan-induced diabetic rabbits. Cardiovasc Ther 32(4): 178–183. DOI: 10.1111/1755-5922.12079.

Liu X, Zhang W, Luo J, Shi W, Zhang X, Li Z, et al. (2023b). TRIM21 deficiency protects against atrial inflammation and remodeling post myocardial infarction by attenuating oxidative stress. Redox Biol 62: 102679. DOI: 10.1016/j.redox.2023.102679.

Lv W, Zhang L, Cheng X, Wang H, Qin W, Zhou X, Tang B (2020). Apelin Inhibits Angiotensin II-Induced Atrial Fibrosis and Atrial Fibrillation via TGF-β1/Smad2/α-SMA Pathway. Front Physiol 11: 583570. DOI: 10.3389/fphys.2020.583570.

Nattel S (2017). Molecular and Cellular Mechanisms of Atrial Fibrosis in Atrial Fibrillation. JACC Clin Electrophysiol 3(5): 425–435. DOI: 10.1016/j.jacep.2017.03.002.

Park J, Song H, Moon S, Kim Y, Cho S, Han K, et al. (2024). Cardiometabolic benefits of fenofibrate in heart failure related to obesity and diabetes. Cardiovasc Diabetol 23(1): 343. DOI: 10.1186/s12933-024-02417-6.

Pedro B, Fontes-Sousa ASP, Gelzer AR (2020). Diagnosis and management of canine atrial fibrillation. Vet J 265: 105549. DOI: 10.1016/j.tvjl.2020.105549.

Qin X, Liu P, Jin L, Zhu K, Yang Y, Hou Z, et al. (2024). Exerkine β-aminoisobutyric acid protects against atrial structural remodeling and atrial fibrillation in obesity via activating AMPK signaling and improving insulin sensitivity. Biomed Pharmacother 171: 116137. DOI: 10.1016/j.biopha.2024.116137.

Qing Y, Dong X, Hongli L, Yanhui L (2018). Berberine promoted myocardial protection of postoperative patients through regulating myocardial autophagy. Biomed Pharmacother 105: 1050–1053. DOI: 10.1016/j.biopha.2018.06.088.

Ramos-Mondragón R, Lozhkin A, Vendrov AE, Runge MS, Isom LL, Madamanchi NR (2023). NADPH Oxidases and Oxidative Stress in the Pathogenesis of Atrial Fibrillation. Antioxidants (Basel) 12(10): 1833. DOI: 10.3390/antiox12101833.

Rillig A, Magnussen C, Ozga AK, Suling A, Brandes A, Breithardt G, et al. (2021). Early Rhythm Control Therapy in Patients With Atrial Fibrillation and Heart Failure. Circulation 144(11): 845–858. DOI: 10.1161/CIRCULATIONAHA.121.056323.

Sagris M, Vardas EP, Theofilis P, Antonopoulos AS, Oikonomou E, Tousoulis D (2021). Atrial Fibrillation: Pathogenesis, Predisposing Factors, and Genetics. Int J Mol Sci 23(1): 6. DOI: 10.3390/ijms23010006.

Sharma P, Raju B, Narendra G, Sapra B, Silakari O (2022). Molecular Docking, Dynamics, and WaterSwap Analysis to Identify Anti-aggregating Agents of Insulin and IFN-β. Appl Biochem Biotechnol 194(7): 3261–3279. DOI: 10.1007/s12010-022-03881-0.

Shu H, Cheng J, Li N, Zhang Z, Nie J, Peng Y, et al. (2023). Obesity and atrial fibrillation: a narrative review from arrhythmogenic mechanisms to clinical significance. Cardiovasc Diabetol 22(1): 192. DOI: 10.1186/s12933-023-01913-5.

Song J (2022). The Chinese burden of atrial fibrillation review of atrial fibrillation studies in China. Ann Noninvasive Electrocardiol 27(6): e12957. DOI: 10.1111/anec.12957.

Song D, Hao J, Fan D (2020). Biological properties and clinical applications of berberine. Front Med 14(5): 564–582. DOI: 10.1007/s11684-019-0724-6.

Souza-Neto FV, Islas F, Jiménez-González S, Luaces M, Ramchandani B, Romero-Miranda A, et al. (2022). Mitochondrial Oxidative Stress Promotes Cardiac Remodeling in Myocardial Infarction through the Activation of Endoplasmic Reticulum Stress. Antioxidants (Basel) 11(7): 1232. DOI: 10.3390/antiox11071232.

Sun Z, Wang Y, Pang X, Wang X, Zeng H (2023). Mechanisms of polydatin against spinal cord ischemia-reperfusion injury based on network pharmacology, molecular docking and molecular dynamics simulation. Bioorg Chem 140: 106840. DOI: 10.1016/j.bioorg.2023.106840.

Wang D, Wang X, Yang T, Tian H, Su Y, Wang Q (2023). Long Non-Coding RNA Dancr Affects Myocardial Fibrosis in Atrial Fibrillation Mice via the MicroRNA-146b-5p/Smad5 Axis. Acta Cardiol Sin 39(6): 841–853. DOI: 10.6515/ACS.202311_39(6).20230619B.

Wang K, Feng X, Chai L, Cao S, Qiu F (2017a). The metabolism of berberine and its contribution to the pharmacological effects. Drug Metab Rev 49(2): 139–157. DOI: 10.1080/03602532.2017.1306544.

Wang M, Zhou F, Luo Y, Deng X, Chen X, Yi Q (2024). The transcription factor PPARA mediates SIRT1 regulation of NCOR1 to protect damaged heart cells. Cardiovasc Diagn Ther 14(5): 832–847. DOI: 10.21037/cdt-24-101.

Wang Z, Tang Z, Zhu W, Ge L, Ge J (2017b). Efficacy and safety of traditional Chinese medicine on thromboembolic events in patients with atrial fibrillation: A systematic review and meta-analysis. Complement Ther Med 32: 1–10. DOI: 10.1016/j.ctim.2017.03.006.

Xu H, Li O, Kim D, Xue M, Bao Z, Yang F (2024). Aged microbiota exacerbates cardiac failure by PPARα/PGC1α pathway. Biochim Biophys Acta Mol Basis Dis 1870(7): 167271. DOI: 10.1016/j.bbadis.2024.167271.

Yang KT, Chao TH, Wang IC, Luo YP, Ting PC, Lin JH, Chang JC et al. (2022). Berberine protects cardiac cells against ferroptosis. Tzu Chi Med J 34(3): 310–317. DOI: 10.4103/tcmj.tcmj_236_21.

Yuan M, Gong M, He J, Xie B, Zhang Z, Meng L, et al. (2022). IP3R1/GRP75/VDAC1 complex mediates endoplasmic reticulum stress-mitochondrial oxidative stress in diabetic atrial remodeling. Redox Biol 52: 102289. DOI: 10.1016/j.redox.2022.102289.

Zhang J, Wang G, Shi Y, Liu X, Liu S, Chen W, et al. (2024). Growth differentiation factor 11 regulates high glucose-induced cardiomyocyte pyroptosis and diabetic cardiomyopathy by inhibiting inflammasome activation. Cardiovasc Diabetol 23(1): 160. DOI: 10.1186/s12933-024-02258-3.

Zhao J, Yu L, Xue X, Xu Y, Huang T, Xu D, et al. (2023). Diminished β7 nicotinic acetylcholine receptor (α7nAChR) rescues amyloid-induced atrial remodeling by oxi-CaMKII/MAPK/AP-1 axis-mediated mitochondrial oxidative stress. Redox Biol 59: 102594. DOI: 10.1016/j.redox.2022.102594.

Zhou ZW, Zheng HC, Zhao LF, Li W, Hou JW, Yu Y, et al. (2015). Effect of berberine on acetylcholine-induced atrial fibrillation in rabbit. Am J Transl Res 7(8): 1450–1457.

Zhu X, Bian H, Wang L, Sun X, Xu X, Yan H, et al. (2019). Berberine attenuates nonalcoholic hepatic steatosis through the AMPK-SREBP-1c-SCD1 pathway. Free Radic Biol Med 141: 192–204. DOI: 10.1016/j.freeradbiomed.2019.06.019.